

# THREE-WAY ARRAY ANALYSIS ON POLARIZED SIGNALS FOR DIRECTION-FINDING AND BLIND SOURCE SEPARATION

Xijing Guo <sup>\*,\*\*</sup> Sebastian Miron <sup>\*</sup> David Brie <sup>\*</sup>

<sup>\*</sup> Centre de Recherche en Automatique de Nancy (CRAN, UMR 7039,  
Nancy-University, CNRS), Faculté des sciences et techniques, BP 239,  
54506 Vandœuvre Cedex, France

<sup>\*\*</sup> Dept. Information and Communication Engineering,  
Xi'an Jiaotong University,  
710049 Xi'an, China

Abstract: By performing Parallel Factor (PARAFAC) analysis over the observations from an electromagnetic vector sensor array, we present a novel way for simultaneous blind source separation and direction-finding (DF) of polarized signals. Identifiability of this model is studied for the efficiency of blind source separation and the performance is shown to approach that of non-blind estimation. Numerical results show that the proposed algorithm can achieve even more accurate estimation on direction-of-arrival (DOA) compared to MUSIC-like algorithms for an array having a small number of sensors.

## 1. INTRODUCTION

Blind source separation is an ill-posed inverse problem, and hence needs additional information to ensure the identifiability of the instantaneous mixture model. Usually, restrictive constraints, such as independence, sparseness or positiveness (Jutten and Babaize-Zadeh, 2006) are imposed on the sources in order to regularize the problem. Another way to ensure the identifiability is to add diversity schemes, leading to the analysis of multi-way array. In that framework, the PARAFAC model was first used in telecommunications by (Sidiropoulos *et al.*, 2000a). Different types of diversity schemes are brought into the literature, such as code diversity (Sidiropoulos *et al.*, 2000a), multi-array diversity (Sidiropoulos *et al.*, 2000b), time block diversity (Rong *et al.*, 2005). Nevertheless, the use of sub-arrays is limited by the physical size of the receiver, and that of temporal sub-blocks needs either an extension of the observation period, or a sharply increased sample rate.

Following the recent development of the electromagnetic vector-sensor technology, it is now possible to consider polarization as an additional diversity as proposed by (Zhang and Xu, 2007). An electromagnetic

sensor is composed of 6 spatially collocated but diversely polarized antennas, measuring all 6 components of the incident electromagnetic field (Nehorai *et al.*, 1999). In this paper, we address the problem of identifiability of the PARAFAC model using polarization diversity. And we precisely state the constraints, under which this model is identifiable. We also illustrate by simulations the advantages of using the PARAFAC decomposition for jointly estimating the source signals and their DOAs. The performances are compared to those of non-blind source separation methods (Weiss and Friedlander, 1993), as well as high resolution vector sensor array processing algorithms (Zoltowski and Wong, 2000).

## 2. DATA MODEL

Consider a uniform array built up with  $M$  identical sensors spaced by  $\Delta x$  along the  $x$ -axis, collecting narrow-band signals emitted from  $N$  ( $N \leq M$  and known *a priori*) spatially distinct far-field sources. For the  $n$ th incoming wave, the DOA is determined by the elevation angle  $\theta_n \in [0, \pi]$  (measured from  $+z$ -

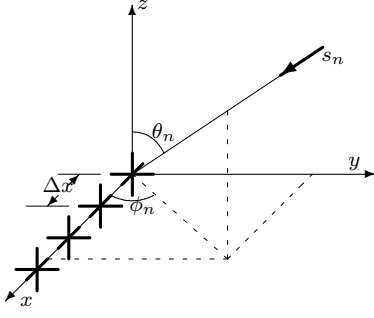


Fig. 1. The Vector Sensor Array

axis) and the azimuth angle  $\phi_n \in [0, \pi)^1$  (measured from  $+x$ -axis), as shown in Fig.1. Under the far-field assumption, the steering vector of the sensor array concerning the  $n$ th impinging wave can be modeled in a Vandermonde structure as

$$\mathbf{a}_n \triangleq [1, a_n, \dots, a_n^{M-1}]^T, \quad (1)$$

where  $a_n = \exp(jk_0 \Delta x \sin \theta_n \cos \phi_n)$  is the inter-sensor phase shift and  $k_0$  is the wave number of the electromagnetic wave.

Suppose the signals are completely polarized, and the propagation takes place in an isotropic, homogeneous medium. A  $2 \times 1$  complex vector

$$\mathbf{g}_n = \begin{bmatrix} \cos \alpha_n & -\sin \alpha_n \\ \sin \alpha_n & \cos \alpha_n \end{bmatrix} \begin{bmatrix} j \sin \beta_n \\ \cos \beta_n \end{bmatrix}$$

is used to describe the polarization state of the  $n$ th signal in terms of the orientation angle  $\alpha_n \in (-\pi/2, \pi/2]$  and the ellipticity angle  $\beta_n \in [-\pi/4, \pi/4]$  (Compton, 1981). If the  $n$ th incoming wave has unit power, the electric- and magnetic-fields,  $\mathbf{e}_n$  and  $\mathbf{h}_n$ , measured by each vector-sensor can be put together in a  $6 \times 1$  vector  $\mathbf{b}_n$  (Nehorai *et al.*, 1999) in Cartesian coordinates:

$$\mathbf{b}_n \triangleq \begin{bmatrix} \mathbf{e}_n \\ \mathbf{h}_n \end{bmatrix} = \begin{bmatrix} \cos \theta_n \cos \phi_n & -\sin \phi_n \\ \cos \theta_n \sin \phi_n & \cos \phi_n \\ -\sin \theta_n & 0 \\ -\sin \phi_n & -\cos \theta_n \cos \phi_n \\ \cos \phi_n & -\cos \theta_n \sin \phi_n \\ 0 & \sin \theta_n \end{bmatrix} \mathbf{g}_n. \quad (2)$$

For notation compactness, we use  $\mathbf{\Pi}_n$  to denote the  $6 \times 2$  matrix on the righthand side of (2), which is referred to the steering matrix of a vector-sensor in (Nehorai *et al.*, 1999), hence we have  $\mathbf{b}_n = \mathbf{\Pi}_n \mathbf{g}_n$ .

Neglect the mutual coupling effects inner-<sup>2</sup> or intersensors, and focus on the  $m$ th ( $m = 1, 2, \dots, M$ ) vector-sensor, which outputs 6 parallel discrete-time baseband-equivalent data flows simultaneously. Let  $p$

<sup>1</sup> We assume the sources are all coming from the  $+y$  side of the  $x-z$  plane.

<sup>2</sup> This approximation is justifiable since small mutual coupling effects among the vector's six components were reported by Flam & Russell, Inc., Horsham, PA; see (Wong and Zoltowski, 2000).

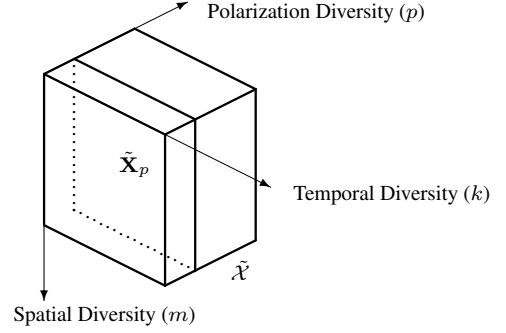


Fig. 2. Illustration of Data Structure

( $p = 1, 2, \dots, 6$ ) index the six field components respectively. The  $p$ th output,  $x_{m,p}(t_k)$  ( $k = 1, 2, \dots, K$  and  $K \geq N$ ), is obtained by summing up all the contributions from the  $N$  wavefronts, *i.e.*,

$$x_{m,p}(t_k) = \sum_{n=1}^N a_n^{m-1} [\mathbf{b}_n]_p s_n(t_k) + n_{m,p}(t_k), \quad (3)$$

where

- $[\cdot]_p$  the  $p$ th component of a vector;
- $s_n(t_k)$  temporal samples of the  $n$ th source signal;
- $n_{m,p}(t_k)$  additive white noise, i.i.d. for  $m, p$ , and  $k$ .

Let us define respectively

$$\mathbf{A} \triangleq [\mathbf{a}_1, \dots, \mathbf{a}_N] \quad (4)$$

$$\mathbf{B} \triangleq [\mathbf{b}_1, \dots, \mathbf{b}_N] \quad (5)$$

$$\mathbf{S} \triangleq \begin{bmatrix} s_1(t_1) & \dots & s_N(t_1) \\ \vdots & \ddots & \vdots \\ s_1(t_K) & \dots & s_N(t_K) \end{bmatrix} \quad (6)$$

as the  $M \times N$  array response, the  $6 \times N$  polarization-dependent response of each vector-sensor, and  $K \times N$  source signal matrix. We also define the  $M \times K$  matrix

$$\tilde{\mathbf{X}}_p \triangleq \begin{bmatrix} x_{1,p}(t_1) & \dots & x_{1,p}(t_K) \\ \vdots & \ddots & \vdots \\ x_{M,p}(t_1) & \dots & x_{M,p}(t_K) \end{bmatrix} \quad (7)$$

collecting the compact data measured from the  $p$ th component of all  $M$  sensors. If the entire data set  $\{\tilde{\mathbf{X}}_p \mid p = 1, \dots, 6\}$  is organized in an  $M \times K \times 6$  tensor  $\tilde{\mathcal{X}}$  as illustrated in Fig.2, the signal model formulated in (3) can be re-expressed in the matrix form as

$$\tilde{\mathbf{X}}_p = \mathbf{A} \mathbf{D}_p(\mathbf{B}) \mathbf{S}^T + \mathbf{N}_p, \quad p = 1, \dots, 6, \quad (8)$$

where

$$\mathbf{D}_p(\mathbf{B}) = \begin{bmatrix} b_{p1} & & 0 \\ & \ddots & \\ 0 & & b_{pN} \end{bmatrix} \quad (9)$$

denotes the diagonal matrix with the  $p$ th row of  $\mathbf{B}$  as its diagonal, and  $b_{pn} \triangleq [\mathbf{b}_n]_p$  is the  $(p, n)$ th entry of matrix  $\mathbf{B}$ .

$$\Sigma = \sqrt{[\sin \theta_1 \sin \theta_2 + (1 + \cos \theta_1 \cos \theta_2) \cos \Delta \phi]^2 + (\cos \theta_1 + \cos \theta_2)^2 \sin^2 \Delta \phi} \quad (15)$$

$$\epsilon = \tan^{-1} \frac{(\cos \theta_1 + \cos \theta_2) \sin \Delta \phi}{\sin \theta_1 \sin \theta_2 + (1 + \cos \theta_1 \cos \theta_2) \cos \Delta \phi} \quad (16)$$

Equations (8) and (9) clearly express a 3-way PARAFAC structure of the recorded data (Harshman, 1981).

### 3. IDENTIFIABILITY AND ESTIMATION PERFORMANCE

#### 3.1 Identifiability of Noise-Free Data

Let  $\mathcal{X} \triangleq \tilde{\mathcal{X}} - \mathcal{N}$  be the noise-free data, then the  $p$ th slice,  $\mathbf{X}_p$ , is equal to

$$\mathbf{X}_p = \mathbf{A} \mathbf{D}_p(\mathbf{B}) \mathbf{S}^T, \quad p = 1, \dots, 6, \quad (10)$$

and  $\mathcal{X}$  can be unfolded into a  $6M \times K$  matrix:

$$\begin{bmatrix} \mathbf{X}_1 \\ \vdots \\ \mathbf{X}_6 \end{bmatrix} = \begin{bmatrix} \mathbf{A} \mathbf{D}_1(\mathbf{B}) \mathbf{S}^T \\ \vdots \\ \mathbf{A} \mathbf{D}_6(\mathbf{B}) \mathbf{S}^T \end{bmatrix} = (\mathbf{B} \odot \mathbf{A}) \mathbf{S}^T \quad (11)$$

where  $\odot$  is the Khatri-Rao (column-wise Kronecker) product (Sidiropoulos *et al.*, 2000a).

To obtain a unique and valid solution for the inverse problem posed in (11), identifiability must be studied before estimating  $\mathbf{A}$ ,  $\mathbf{B}$  and  $\mathbf{S}$  for the DOA information and source signal recovery. Kruskal's condition is a sufficient condition for unique PARAFAC decomposition, relying on the concept defined as Kruskal-rank or  $k$ -rank (Kruskal, 1977).

*Definition:* Given a matrix  $\mathbf{A} \in \mathbb{C}^{I \times J}$ , if every linear combination of  $l$  columns has full column rank, but this condition does not hold for  $l + 1$ , then the  $k$ -rank of  $\mathbf{A}$  is  $l$ , written as  $k_{\mathbf{A}} = l$ .

Note that  $k_{\mathbf{A}} \leq \text{rank}(\mathbf{A}) \leq \min(I, J)$ , and both the equalities hold when  $\text{rank}(\mathbf{A}) = J$ .

Kruskal's condition was first established for trilinear decomposition of real-valued arrays (Kruskal, 1977), and later extended by (Sidiropoulos *et al.*, 2000a) to complex-valued cases. In our context, this uniqueness condition can be formulated as follows.

*Kruskal's condition:* Consider a 3-way array  $\mathcal{X}$  structured as in (11). Decomposition into three matrices  $\mathbf{A}$ ,  $\mathbf{B}$  and  $\mathbf{S}$  is unique up to column permutation and scaling ambiguities, if but not necessarily

$$k_{\mathbf{A}} + k_{\mathbf{B}} + k_{\mathbf{S}} \geq 2(N + 1). \quad (12)$$

In separation and recovery of two sources, if one source comes from  $(\theta, \phi)$  and the other from  $(\pi - \theta, \phi)$ , the linear independence between  $\mathbf{A}$ 's columns is violated and thus degrades the performance. An  $L$ -shaped array is herein adopted to eliminate this ambiguity. The  $L$ -shaped array involved here is constructed by posing  $M_z$  sensors along the  $+z$ -axis and

the  $M - M_z$  others along the  $+x$ -axis, resulting in the following expression for the steering vector:

$$\mathbf{a}_n = \begin{bmatrix} e^{j(M_z - 1)k_0 \Delta x \cos \theta_n} \\ \vdots \\ e^{jk_0 \Delta x \cos \theta_n} \\ 1 \\ e^{jk_0 \Delta x \sin \theta_n \cos \phi_n} \\ \vdots \\ e^{j(M - M_z)k_0 \Delta x \sin \theta_n \cos \phi_n} \end{bmatrix}. \quad (13)$$

Now we make the following assumptions on the mixture of unknown sources in order to satisfy Kruskal's condition.

- (A1) Sources have distinct DOA, *i.e.*, any two sources have at least one different parameter, either  $\theta$  or  $\phi$ .
- (A2) Each source sequence is drawn from an unknown stochastic process of continuous distribution.

Due to the column structure of  $\mathbf{A}$  as shown in (13), it is straightforward to show that (A1) guarantees  $\text{rank}(\mathbf{A}) = N$  and hence  $k_{\mathbf{A}} = N$ . Since (A2) imposes the full rank condition on the signal matrix  $\mathbf{S}$ , it follows that  $k_{\mathbf{S}} = N$ . If  $k_{\mathbf{B}} \geq 2$  is further verified, then Kruskal's condition can be satisfied to achieve unique PARAFAC decomposition. We will prove this by contradiction.

Assume  $k_{\mathbf{B}} < 2$ , then there must exist at least one pair of linear dependent columns, namely  $\mathbf{b}_1, \mathbf{b}_2$ , so that

$$|\mathbf{b}_1^H \mathbf{b}_2| = \|\mathbf{b}_1\| \|\mathbf{b}_2\|. \quad (14)$$

Let  $(\theta_1, \phi_1)$  and  $(\theta_2, \phi_2)$  denote the DOA of any two sources, and assume  $\phi_2 > \phi_1$  with the difference  $\Delta \phi = \phi_2 - \phi_1$ . With  $\Sigma$  and  $\epsilon$  given by (15) and (16) respectively at the top of this page after tedious computations,

$$\mathbf{\Pi}_1^H \mathbf{\Pi}_2 = \Sigma \begin{bmatrix} \cos \epsilon & -\sin \epsilon \\ \sin \epsilon & \cos \epsilon \end{bmatrix} \quad (17)$$

can be understood as a scaling and rotation operation over an incoming wave's polarization, where  $\Sigma$  is the scaling factor and  $\epsilon$  is the rotation factor. Define  $\Omega_{\epsilon}$  that satisfies  $\cos \Omega_{\epsilon} =$

$\sin 2\beta_1 \sin 2\beta_2 + \cos 2\beta_1 \cos 2\beta_2 \cos 2(\alpha_2 - \alpha_1 + \epsilon)$  and denote  $\Omega_0 = \Omega_{\epsilon}$  when  $\epsilon = 0$ , which is the polarization separation<sup>3</sup> defined in (Compton, 1981),

<sup>3</sup> Polarization separation is defined when two sources have the same DOA. However, for most occasions when two sources have distinct DOAs,  $\Sigma/\Sigma_{\max}$  reflects the angle between the two sources' wavefronts, and  $\epsilon$  depicts the angular distance between their corresponding electric-/magnetic- fields, so that we can still define their polarization separation as if they were from the same DOA.

then we have

$$|\mathbf{b}_1^H \mathbf{b}_2| = |\mathbf{g}_1^H \mathbf{\Pi}_1^H \mathbf{\Pi}_2 \mathbf{g}_2| = \Sigma \sqrt{(1 + \cos \Omega_\epsilon)/2}. \quad (18)$$

Since  $\Sigma$  is defined for  $\theta_1, \theta_2 \in [0, \pi]$  and  $\Delta\phi \in [0, \pi]$ , the maximum of  $\Sigma$  is achieved only if the partial derivatives

$$\frac{\partial \Sigma}{\partial \theta_1} = 0, \quad \frac{\partial \Sigma}{\partial \theta_2} = 0, \quad \frac{\partial \Sigma}{\partial \Delta\phi} = 0,$$

which result in  $\Sigma_{\max} = 2$ , when  $(\theta_1, \phi_1) = (\theta_2, \phi_2)$  or  $\theta_1 = \theta_2 = 0/\pi$  if  $\Delta\phi \neq 0$ , *i.e.*, the DOAs of the sources are identical; hence  $\|\mathbf{b}_2\| = \|\mathbf{b}_1\| = \sqrt{|\mathbf{b}_1^H \mathbf{b}_1|} = \Sigma_{\max}^{1/2}$ . On the contrary, when sources have distinct DOAs, *i.e.*, (A1) holds, (18) yields

$$|\mathbf{b}_1^H \mathbf{b}_2| = \Sigma \sqrt{(1 + \cos \Omega_\epsilon)/2} < \Sigma_{\max} = \|\mathbf{b}_1\| \|\mathbf{b}_2\|, \quad (19)$$

which contradicts (14) and fulfils the proof of  $k_{\mathbf{B}} \geq 2$ .

In general, assumptions (A1) and (A2) can sufficiently satisfy Kruskal's condition (12) and ensure the proposed method identifiable for most occasions.

### 3.2 Noise Effects on Estimation Performance

Define the average input SNR at the receiver as in (Sidiropoulos *et al.*, 2000a)

$$\text{SNR} = 10 \log_{10} \frac{\|\mathcal{X}\|_F^2}{E\|\mathcal{N}\|_F^2} \quad (20)$$

where  $\|\cdot\|_F$  stands for the Frobenius norm, and  $E(\cdot)$  denotes the statistical expectation. Note that the power of source signals  $\|\mathbf{S}\|_F^2$  is determined by the transmitters, thus

$$\|\mathcal{X}\|_F = \|(\mathbf{B} \odot \mathbf{A}) \mathbf{S}^T\|_F \leq \|\mathbf{B} \odot \mathbf{A}\|_F \cdot \|\mathbf{S}\|_F \quad (21)$$

and equality holds if only  $\mathbf{B} \odot \mathbf{A}$  has all orthogonal columns, that is,

$$(\mathbf{B} \odot \mathbf{A})^H (\mathbf{B} \odot \mathbf{A}) = (\mathbf{B}^H \mathbf{B}) \circ (\mathbf{A}^H \mathbf{A}) \propto \mathbf{I}_N, \quad (22)$$

where  $\circ$  is the Hadamard (element-wise) product.

Restricted by  $\|\mathbf{A}\|_F = M\sqrt{N}$  and  $\|\mathbf{B}\|_F = \Sigma_{\max} \sqrt{N} = 2\sqrt{N}$ , (22) holds only if both  $\mathbf{A}$  and  $\mathbf{B}$  are orthogonal, and the maximum of  $\|\mathcal{X}\|_F$  can be achieved, written as

$$\max_{\mathbf{A}, \mathbf{B}} \|\mathcal{X}\|_F = \max_{\mathbf{A}, \mathbf{B}} \|\mathbf{B} \odot \mathbf{A}\|_F \cdot \|\mathbf{S}\|_F = 2M\sqrt{N} \|\mathbf{S}\|_F. \quad (23)$$

Comparing (23) with (20), it indicates, given the same power of source signals and the same noise level, reducing the inner-products between the columns of  $\mathbf{A}$  and those of  $\mathbf{B}$  can increase the average input SNR of the observations, and hence improves the blind source separation performance.

### 3.3 Estimation Algorithm

The Alternating Least Squares (ALS) regression algorithm is the principal approach for PARAFAC decomposition of the multi-way tensors. The algorithm

alternatively updates a subset of parameters using the remaining subsets estimated previously under the least mean square (LMS) criterium, and repeats it until convergence. However, the convergence of this algorithm is linear and sensitive to local minima. Based on ALS, the COMFAC algorithm was proposed in (Bro *et al.*, 1999) to achieve fast, accurate convergence for factorization of trilinear complex-valued tensors through more sophisticated initializations, and herein adopted in this paper for estimating and separating the three matrices, yielding the estimates  $\hat{\mathbf{A}}$ ,  $\hat{\mathbf{B}}$  and  $\hat{\mathbf{S}}$  respectively.

The normalized Poynting vector of the  $n$ th impinging wave, derived simply from a cross product between its electric- and magnetic-field measurements, is collinear to the vector of three direction cosines that exactly depicts the DOA of the  $n$ th source (Wong and Zoltowski, 2000), expressed mathematically as

$$\mathbf{p}_n \triangleq \mathbf{e}_n \times \mathbf{h}_n^* = \begin{bmatrix} \sin \theta_n \cos \phi_n \\ \sin \theta_n \sin \phi_n \\ \cos \theta_n \end{bmatrix} \quad (24)$$

where  $\mathbf{e}_n, \mathbf{h}_n$  are the normalized electric- and magnetic-field vectors respectively presented in (2). Note that, after PARAFAC decomposition when the electric- and magnetic-field vector of the  $n$ th source are eventually separated from each other, concatenated and reserved in a corresponding column of  $\hat{\mathbf{B}}$ , it is straightforward to obtain the estimates of the Poynting vectors for each source and hence their DOAs. Slightly abusing the notations, we replace the 3 direction cosines by

$$\boldsymbol{\kappa} = \begin{bmatrix} u \\ v \\ w \end{bmatrix} = \begin{bmatrix} \sin \theta \cos \phi \\ \sin \theta \sin \phi \\ \cos \theta \end{bmatrix} \quad (25)$$

which can be estimated by optimizing

$$\min_{\|\boldsymbol{\kappa}\|=1} \{ \|\mathbf{a}(\boldsymbol{\kappa}) - \hat{\mathbf{a}}_n\| + \lambda \|\boldsymbol{\kappa} - \Re\{\hat{\mathbf{p}}_n\}\| \} \quad (26)$$

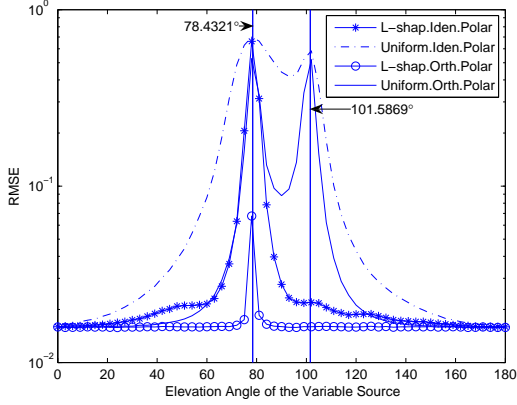
where  $\Re\{\cdot\}$  stands for the real part,  $\lambda$  is a weighting factor,  $\hat{\mathbf{a}}_n$  and  $\hat{\mathbf{p}}_n$  are the estimates of  $\mathbf{a}_n$  and  $\mathbf{p}_n$  obtained previously. In contrast to  $\mathbf{p}_n$ , the estimate  $\hat{\mathbf{p}}_n$  is normally complex-valued due to the noise, which explains the use of  $\Re\{\hat{\mathbf{p}}_n\}$  in (26).

## 4. SIMULATIONS

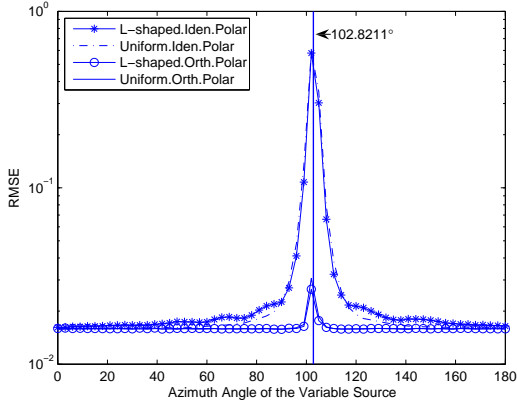
In this section, various Monte Carlo simulations are designed to evaluate the performance of the PARAFAC based algorithm on different aspects. Every simulation experiences  $L = 500$  independent trials, and the noise is assumed to be Gaussian.

### 4.1 Source Separation

The performance of  $L$ -shaped sensor array on blind source separation is compared with that of uniform



(a)  $\phi_1 = \phi_2 = 102.8^\circ$  varying  $\theta_2$



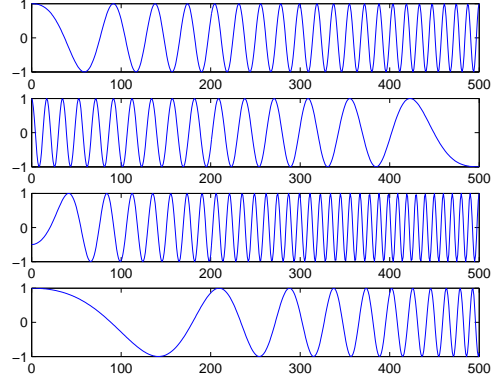
(b)  $\theta_1 = \theta_2 = 78.4^\circ$  varying  $\phi_2$

Fig. 3. RMSE of Signal Estimation vs. Sources Angular Separation

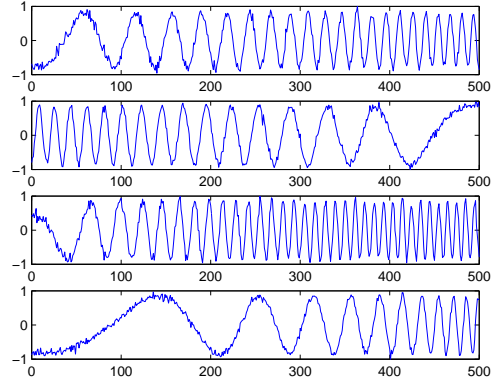
array in terms of the root mean square error (RMSE), as given by

$$\text{RMSE} = \sqrt{\frac{1}{LKN} \sum_{l=1}^L \|\mathbf{S} - \hat{\mathbf{S}}_l\|_F^2}, \quad (27)$$

where  $\hat{\mathbf{S}}_l$  is the estimate of  $\mathbf{S}$  obtained in the  $l$ th trial. A number of 13 sensors are used for both types of array.  $K = 50$  snapshots are used, and SNR is 20dB for all these simulations. For evaluation purpose, a greedy least squares ( $\hat{\mathbf{S}}_l, \mathbf{S}$ )-column matching algorithm (Sidiropoulos *et al.*, 2000a) is applied to resolve the permutation ambiguities. The results are shown in Fig.3. One source is nominated the reference source, which has a set of fixed parameters as  $\theta_1 = 78.4^\circ$ ,  $\phi_1 = 102.8^\circ$ ,  $\alpha_1 = 35.8^\circ$ , and  $\beta_1 = 32.9^\circ$ ; while the other one, namely the variable source, varies on a different aspect of these parameters for each simulation. Fig.3(a) shows the advantage of using  $L$ -shaped array over the uniform array in eliminating the ambiguity of the two sources having supplementary elevation angles, as well as reducing that of inadequate angular separation along the elevation angle direction. Fig.3(b) shows the performance as the variable source varying with respect to the azimuth angle.



(a) Original Sources



(b) Estimated Signals

Fig. 4. Wave-Preserving Character on Separation of 4 Different Chirp Signals

Polarization effects are also concerned and illustrated in Fig.3. Comparing the curves of identically polarized sources with those of orthogonally polarized, it shows that polarization separation plays an auxiliary role in the RMSE performance of blind source separation regarding to the sources angular separation. Distinct polarizations can yield evident enhancement in performance only if lacking of angular separation between the two sources. From (18), when two sources are very close to each other, we have  $\epsilon \rightarrow 0$ ,  $\Sigma \rightarrow \Sigma_{\max}$ , and  $|\mathbf{b}_1^H \mathbf{b}_2| \approx \Sigma_{\max} \sqrt{(1 + \cos \Omega_0)/2}$ , which means polarization separation determines the orthogonality of  $\mathbf{B}$ 's columns and hence the performance; otherwise, when there is sufficient spatial separation, this effect is restrained and limited on the scale of  $10^{-3}$  on the RMSE performance.

Experimental results are presented in Fig.4 to illustrate the wave preserving character of our algorithm. The sources are chosen as 4 different types of chirp signals that can not be easily separated by means of classical filtering. Fig.4(a) shows the original sources and Fig.4(b) lists the estimated sources after eliminating the permutation ambiguity. These recovered signals well fit the original sources shown in Fig.4(a), except for some  $180^\circ$  phase shifts introduced by the complex-valued scalings. The explanation for this indetermi-

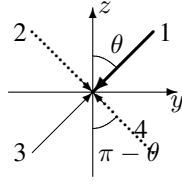


Fig. 5. Illustration of Indeterminacy

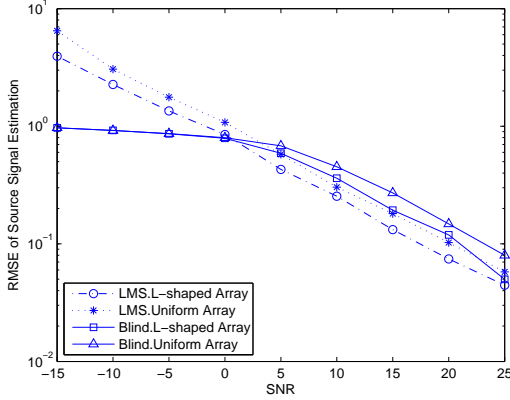


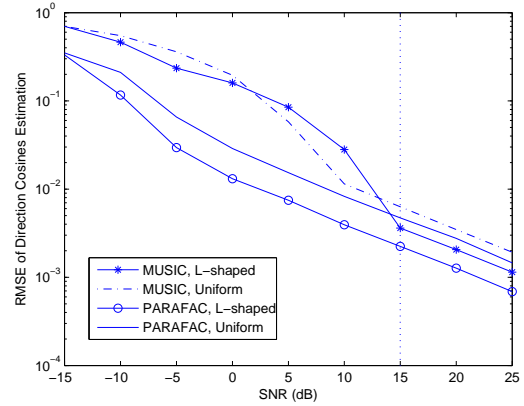
Fig. 6. Blind PARAFAC vs. Nonblind LMS

nacy is illustrated in Fig.5. If “1” is the real DOA of a source, then “2”, “3”, and “4” account for the DOAs of indeterminacy for blind source separation. With  $L$ -shaped array, the ambiguity from “4” can be eliminated and hence “2” as well. Although we assume all the sources are located at the  $+y$  side ( $\phi \in [0, \pi]$ ), the complex scaling ambiguity inherited in blind source separation algorithms can still make the recovered source appear as if it were originated from direction “3”, bringing in the  $180^\circ$  phase shifts in Fig.4(b).

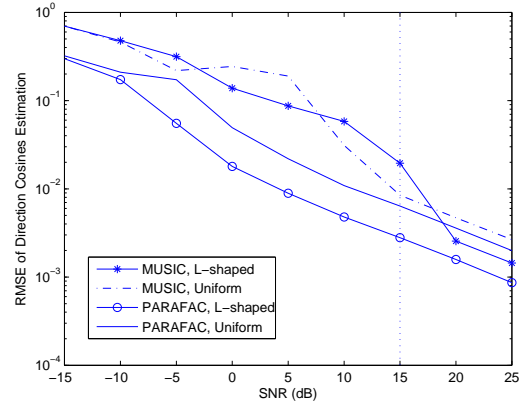
Assume the parameters are all known *a priori* or perfectly estimated, then the source signals can be recovered under LMS criterium (Weiss and Friedlander, 1993). Fig.6 shows an approximation of blind PARAFAC source separation performance to that of non-blind LMS estimators.  $M = 4$  sensors are used to separate  $N = 4$  sources of randomly selected parameters.

#### 4.2 Parameter Estimation

Comparisons on the RMSE performance of estimating direction cosines are conducted between the proposed algorithm and the MUSIC-based algorithm introduced by (Zoltowski and Wong, 2000) using  $M = 4$  sensors. For the MUSIC-based algorithm, we use a more sophisticated initialization strategy of (Wong and Zoltowski, 2000) to acquire faster and more reliable convergence. In our approach, the Nelder-Mead simplex algorithm (Press *et al.*, 1993, ch.10) is used for the optimization of (26) (implemented in MATLAB as “fminsearch” function). Fig.7(a) illustrates the RMSE of  $\|\hat{\kappa}_1 - \kappa_1\|$  using both algorithms when the



(a) from Uncorrelated Sources



(b) from Correlated Sources

Fig. 7. RMSE of D.C. Estimation vs. SNR

sources are uncorrelated, as Fig.7(b) shows the same aspect of estimation performance but using correlated sources, with the correlation matrix given by

$$\begin{bmatrix} 0.6279 & 0.3721 \\ 0.3721 & 0.6279 \end{bmatrix}.$$

All the parameters are randomly selected in these simulations, and we set  $\lambda = 1$  in this paper. On Fig.7(a), where sources are uncorrelated, the proposed algorithm presents better performance than the MUSIC-based approach at low SNRs; even for the high SNR (beyond 20dB) cases, the performance still surpasses that of the MUSIC-based by 3dB. Moreover, an effective PARAFAC decomposition relies on the linear independence among the signal sequences, instead of the more strict assumption of uncorrelated sources for MUSIC-like algorithms. Fig.7(b) clearly shows the stability of using our approach for correlated sources, whereas the performance of the MUSIC-based is degraded by nearly 5dB.

Other than the correlation of the sources, the MUSIC-based algorithm is also sensitive to the sample length of the data, as shown in Fig.8. The RMSE keeps one order of magnitude more than that of the PARAFAC-based algorithm until  $K = 300$ .

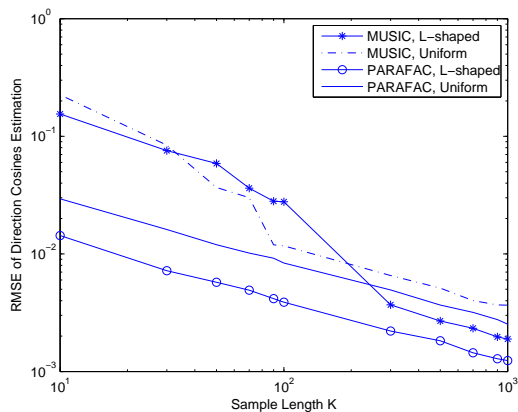


Fig. 8. RMSE of D.C. Estimation vs. Sample Length (K)

## 5. CONCLUSIONS

In this paper, a link has been established between PARAFAC analysis and the vector-sensor array for simultaneous blind polarized source separation and DOA estimation. We proved that, with an  $L$ -shaped array, identifiability can always be achieved as long as the sources have distinct DOAs. Simulation results show that the performance of the proposed algorithm is similar to that of non-blind source separation methods available in the literature. Furthermore, for a small number of sensors, our algorithm outperforms the classical polarized MUSIC algorithm for DOA estimation. In particular, this PARAFAC-based algorithm does not require the statistical independence of sources but rather their linear independence. This allows to handle the challenging case of correlated sources.

Further works would be directed at comparing the DOA estimation performance of the proposed approach to the recent extensions of MUSIC algorithm, such as the quaternion-MUSIC algorithm (Miron *et al.*, 2006). Another point is to investigate the validation of the hypothesis that imposes no mutual coupling across the sensors. Finally, we also aim at extending this multilinear model to the more complicated case of multipath propagation, by studying the possible use of the more general Tucker3 model (Tucker, 1966).

## 6. REFERENCES

- Bro, R., N.D. Sidiropoulos and G.B. Giannakis (1999). A fast least squares algorithm for separating trilinear mixtures. In: *Proc. Int. Workshop Independent Component Analysis and Blind Signal Separation*. Aussois, France.
- Compton, R.T. (1981). The tripole antenna: an adaptive array with full polarization flexibility. *IEEE Trans. Antennas Propagat.*, **AP-29**(6), 944–952.
- Harshman, R.A. (1981). Foundations of the PARAFAC procedure: Model and conditions for an ‘explanatory’ multi-mode factor analysis. *UCLA Working Papers Phonetics*, **16**, 1–84.
- Jutten, C. and M. Babaize-Zadeh (2006). Source separation: Principles, current advances and applications. In: *21st IAR Workshop*. Nancy, France.
- Kruskal, J.B. (1977). Three-way arrays: Rank and uniqueness of trilinear decompositions with application to arithmetic complexity and statistics. *Linear Algebra Applicat.*, **18**, 95–138.
- Miron, S., N. Le Bihan and J.I. Mars (2006). Quaternion MUSIC for vector-sensor array processing. *IEEE Trans. Signal Processing*, **54**(4), 1218–1229.
- Nehorai, A., K.-C. Ho and B.T.G. Tan (1999). Minimum-noise-variance beamformer with an electromagnetic vector sensor. *IEEE Trans. Signal Processing*, **47**(3), 601–618.
- Press, William, Saul Teukolsky, William Vetterling and Brian Flannery (1993). *Numerical Recipes: The Art of Scientific Computing*. 2 ed.. Cambridge University Press.
- Rong, Y., S.A. Vorobyov, A.B. Gershman and N.D. Sidiropoulos (2005). Blind spatial signature estimation via time-varying user power loading and parallel factor analysis. *IEEE Trans. Signal Processing*, **53**(5), 1697–1710.
- Sidiropoulos, N.D., G.B. Giannakis and R. Bro (2000a). Blind PARAFAC receivers for DS-CDMA systems. *IEEE Trans. Signal Processing*, **48**(3), 810–823.
- Sidiropoulos, N.D., R. Bro and G.B. Giannakis (2000b). Parallel factor analysis in sensor array processing. *IEEE Trans. Signal Processing*, **48**(8), 2377–2388.
- Tucker, L.R. (1966). Some mathematical notes on three-mode factor analysis. *Psychometrika*, **31**(3), 279–311.
- Weiss, A.J. and B. Friedlander (1993). Analysis of a signal estimation algorithm for diversity polarized arrays. *IEEE Trans. Signal Processing*, **41**(8), 2628–2638.
- Wong, K.T. and M.D. Zoltowski (2000). Self-initiating MUSIC-based direction finding and polarization estimation in spatio-polarizational beamspace. *IEEE Trans. Antennas Propagat.*, **48**(8), 1235–1345.
- Zhang, X. and D. Xu (2007). Blind PARAFAC signal detection for polarization sensitive array. *EURASIP Journal on Advances in Signal Processing*, **2007**, Article ID 12025, 7 pages.
- Zoltowski, M.D. and K.T. Wong (2000). Closed-form eigenstructure-based direction finding using arbitrary but identical subarrays on a sparse uniform cartesian array grid. *IEEE Trans. Signal Processing*, **48**(8), 2205–2210.